2023 IEEE International Conference on Robotics and Automation (ICRA 2023)
May 29 - June 2, 2023. London, UK

Using a Collaborative Robotic Arm as Human-Machine Interface: System Setup and Application to Pose Control Tasks

Christian A. Braun[1], Ludwig Haide[1], Lars Fischer[1], Sean Kille[1], Balint Varga[1], Simon Rothfuss[1] and Sören Hohmann[1]

***Abstract*— While robotic arms have been used in a vast range of application areas, so far no extensive reports on the utilization as human-machine interface exist. Compared to HMI devices from literature, the robotic arm used in this work (KUKA LBR iiwa 14 R820) features a relatively large workspace and is able to generate force and torque feedback that surpasses the capabilities of literature devices. We describe the setup allowing to use the robotic arm as HMI and analytically determine the optimal initial pose of it based on the manipulability measure of Yoshikawa. To demonstrate that the robotic arm is able to serve as HMI, we report on a comparative study with a state of the art haptic HMI featuring 20 participants. Additionally, two applications from the context of planetary exploration are presented: The first considers the teleoperation of the pan-tilt unit of a lightweight rover unit and illustrates how the large workspace of the HMI benefits the precision of the teleoperation compared to a setup with a smaller workspace. The second experiment showcases the use of the force feedback of the HMI to enable a cooperation between the operator and a supporting path-following automation in a shared control of a simulated ground robot. Both the study and the applications highlight the performance, precision and reliability of our proposed system.**

I. INTRODUCTION

In 2015, Jan Wörner of the European Space Agency proposed the concept of a permanent basis on the moon called *Moon Village* [1]. In the various stages of the development of the Moon Village, robotic assets will be crucial for erecting buildings, setting up infrastructure, transporting equipment, scientific exploration and maintenance tasks [2], [3], [4]. Due to the variety and complexity of tasks required for this endeavor, heterogeneous teams of robots will likely play an important role for its success [5]. While autonomous capabilities of the robotic assets will be crucial, teleoperation by humans is also of importance [6], [7], [8], e.g. if the limits of the autonomous capabilities are reached or a deviation from the automated behaviour is necessary. In such a teleoperated case, a suitable human-machine interface (HMI) is required. In similar applications, dedicated HMIs are currently used [9]. However, as the transportation of one kilogram of payload to the lunar surface costs around $\$1,200,000$ [10], the question arises whether hardware that might be available anyways can be used as an HMI.

Robotic arms have been widely applied e.g. in medicine [11], service robotics [12] or manufacturing and assembly [13]. This variety of application areas stems from their flexible usability, hence they might also be applied in various tasks in a future Moon Village. Robotic arms usually feature the ability to be positioned in multiple degrees of freedom (DOF) as well as sensors to determine the position of their end-effector, thus making them applicable as HMI by merely attaching a suitable handle to the end-effector and mounting them in a convenient height for the operator. Hence, a robotic arm that will likely be available due to a different use-case could increase payload efficiency of the mission by additionally serving as HMI. To the best of our knowledge, there is no report on the application and evaluation of a robotic arm as HMI, thus this work aims to close this gap by reporting on the HMI depicted in Fig. 1.

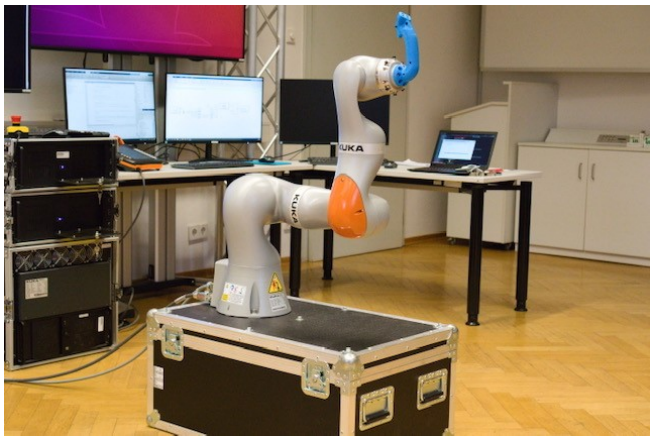

Fig. 1: KUKA LBR iiwa 14 R820 as HMI.

To do so, the remaining paper is organized as follows: In Section II we compare the features of the robotic arm used in this work to existing HMIs. We then describe the setup allowing to use it as an HMI in Section III. Next, the resulting HMI is evaluated in a comparative study as well as in two robotic applications described in Section IV. Subsequently, Section V compiles the findings of this work and gives an outlook on future work.

II. COMPARISON TO THE STATE OF THE ART

While the robotic assets deployed in the context of a Moon Village may be heterogeneous, the teleoperation of the robot pose in the up to three dimensional space is universally relevant to all of them. Due to their importance, we focus on these pose control tasks of up to three rotational plus three translational DOFs. To operate these six DOFs, HMIs that feature six DOFs themselves are of special interest, as

*This work was supported by the Helmholtz Future Project *ARCHES* (Autonomous Robots Helping Modern Societies).

[1]Institute of Control Systems, Karlsruhe Institute of Technology, 76131 Karlsruhe, Germany (christian.braun@kit.edu)

they allow for a direct mapping of one DOF of the HMI to one DOF of the robotic asset. The robotic arm exemplarily investigated in this work, a KUKA LBR iiwa 14 R820 (LBR), features seven DOFs and is thus able to act as six DOF HMI with a kinematic redundancy. Due to the great importance of force feedback in the space exploration context e.g. for telepresence or to provide guidance from a supporting automation, we focus on HMIs featuring meaningful force feedback to enable these applications. Table I analyzes how the LBR compares to established HMI devices with six DOFs and force feedback to evaluate its general suitability to serve as six DOF HMI. Considering the workspaces listed in the third and fourth column, the LBR is able to provide at least the same if not a larger one compared to seven out of the eight literature devices. Only the Phantom Premium 3.0 features a workspace that cannot be enclosed by the robotic arm, even though the overall workspace volume of the LBR exceeds the one of the Phantom Premium 3.0. While the larger workspace volume can be used in applications that allow for movement around the LBR's base, we mostly limited it e.g. to cubes of sizes $350\mathrm{mm} \times 350\mathrm{mm} \times 300\mathrm{mm}$ for a stationary operation. Overall, the workspace of the robotic arm is relatively large compared to the majority literature HMI devices but still reasonable for the application as HMI. Columns five and six of Table I list the maximum forces and torques the HMIs are able to provide e.g. for telepresence or feedback from a supporting automation. The robotic arm exceeds the capabilities of all the literature devices by far, allowing to utilize the whole range forces admissible in human-robot interaction [23]. The comparably small forces and torques applied by literature devices are therefore easily realizable, further underlining the capability of the robotic arm to serve as HMI. At the same time, the abilities of the literature devices make it clear that the reverse does not hold: While a robotic arm may serve as HMI, it will not be possible to utilize an established HMI for most of the application areas of robotic arms as the build of the HMIs is usually too fragile to do so. Hence, this literature analysis supports the idea of increasing payload efficiency by using a robotic arm as HMI.

III. System Setup

In order to achieve the goal of teleoperating a robotic asset using the HMI, two core functionalities have to be implemented: Firstly, the current pose of the robotic arm needs to be mapped to the range of command values of the robotic asset, secondly, suitable wrenches have to be applied to its end-effector e.g. to enable shared control approaches or to generate suitable forces for a telepresence-setting. Both functionalities require communication and thus ideally a common interface with the environment, especially with different robotic assets.

The robot operating system (ROS) [24] is both popular and able to serve as such a common interface, hence we aim at interfacing the HMI to ROS. The LBR is controlled by a KUKA Sunrise Cabinet that allows to run Java applications and provides TCP/IP communication. Even though no interface to ROS is implemented out-of-the-box, a direct interface to ROS could be implemented on the Sunrise Cabinet in principle; however, we choose to use the KST-Toolbox [25] to interface the Sunrise Cabinet to MATLAB via TCP/IP. This allows for using the whole suite of MATLAB-tools for research and development, while additionally providing the ROS-functionalities of MATLAB to further interface the LBR to ROS. Additionally, all application-specific parameterization can be performed in MATLAB while the code on the Sunrise Cabinet remains the same which allows for more rapid development cycles. While using MATLAB does introduce some delay, we measured an average cycle time of $1.9\,\mathrm{ms}$ with a standard deviation of $0.465\,\mathrm{ms}$ for sending one set of set-values to the Sunrise Cabinet via MATLAB and receiving pose data from the Sunrise Cabinet in MATLAB in over 7000 cycles, which is acceptable for the proposed application.

Figure 2 shows an overview of the software components used to operate the HMI. The ROS-network depicted on the left-hand side interfaces the operated robotic asset(s), a visualization e.g. of the camera stream of the robot and the data logging. To prevent bandwidth-issues from influencing other functionalities implemented in MATLAB, both the publishing of commands to the operated robotic asset

TABLE I: Comparison of properties of a KUKA LBR iiwa 14 R820 and literature HMI devices. The sign '-' indicates missing information in references.

Device	Reference	Translational workspace in mm	Rotational workspace in degree	Force Feedback in N	Torque Feedback in Nm
KUKA LBR iiwa 14 R820	[14]	820 outer diameter, 420 inner diameter spherical shell	340 x 340 x 340	140	40
Phantom Premium 3.0	[15]	838 x 584 x 406	297 x 260 x 335	22	0.17
Sigma.7	[16]	190 x 130 ellipsoid	235 x 140 x 200	20	0.4
Delta with gimbal	[17]	150 diameter sphere	140 x 140 x 140	10	0.71
Parallel kinematic machine	[18]	300 diameter sphere	120 x 120 x 360	20	3
Parallel kinematic machine	[19]	110 diameter x 100 height cylinder	-	20	2
Modified Stewart platform	[20]	300 sphere	-	23	-
Modified Stewart platform	[21]	320 x 170 ellipsoid	-	15	-
Delta combination	[22]	-	-	30	

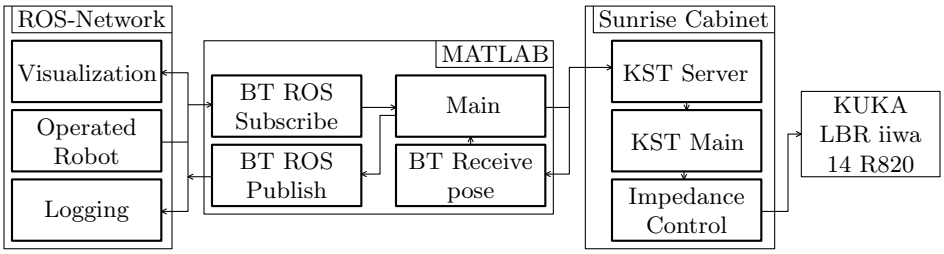

Fig. 2: Overview of the software components used to operate the HMI (BT=Background-Thread).

and subscribing e.g. to measurement data is performed in asynchronous background-threads. The pose of the LBR is acquired through another background-thread that provides its information to the Main script which maps it to commands to the operated robotic asset and computes set-values for the wrenches of the LBR. A KST Server on the Sunrise Cabinet is used to send the set-values to the KST Main script that configures an impedance controller to realize the desired wrenches.

While the mapping of the measured pose-data to the commanded values can easily be performed by a normalization of the measured pose value to the workspace and a subsequent normalization to the expected value range of the commanded values to the operated robotic asset, the generation of a desired wrench vector $\boldsymbol{\mathcal{F}} \in \mathbb{R}^6$ requires more extensive steps.

A. Concept for realizing wrenches

The cartesian impedance control already available on the Sunrise Cabinet allows the LBR to exert wrenches based on the distance of the measured cartesian LBR pose $\boldsymbol{p}_{\mathrm{meas}} \in \mathbb{R}^6$ and a commanded cartesian pose $\boldsymbol{p}_{\mathrm{set}} \in \mathbb{R}^6$:

$$\boldsymbol{\mathcal{F}} = \boldsymbol{C}\left(\boldsymbol{p}_{\mathrm{meas}} - \boldsymbol{p}_{\mathrm{set}}\right) \tag{1}$$

Here, the diagonal matrix $\boldsymbol{C} \in \mathbb{R}^{6\times 6}$ contains the stiffnesses of virtual springs in each of the six DOFs as diagonal elements ($\boldsymbol{C}_{ii} \geq 0, i \in \{1,\ldots,6\}$). As only the diagonal elements of $\boldsymbol{C}$ are populated, each row of (1) can be considered individually. Without limiting the generality of our consideration, we discuss the first row of (1) in the following, all results are analogous for the remaining rows. Please note that we omit the time-dependencies of all variables for better readability.

To generate a desired $\boldsymbol{\mathcal{F}}_x$ at the end-effector of the LBR, suitable parameters $\boldsymbol{C}_{11}$ and $\boldsymbol{p}_{\mathrm{set},x}$ have to be set. While in theory setting $\boldsymbol{C}_{11}$ to a constant non-zero value and solving (1) for $\boldsymbol{p}_{\mathrm{set},x}$ is feasible, we found the haptic experience using the KUKA impedance control to be the smoothest, the closer $\boldsymbol{p}_{\mathrm{set},x}$ was to $\boldsymbol{p}_{\mathrm{meas},x}$. Due to $\boldsymbol{C}_{11}$ being limited to positive values below or equal to $\boldsymbol{C}_{11,\max} = 5000\,\mathrm{Nm}^{-1}$, a maximum deviation of $\boldsymbol{p}_{\mathrm{set},x}$ and $\boldsymbol{p}_{\mathrm{meas},x}$ of $\Delta x_{\max} = 28\,\mathrm{mm}$ is required to achieve the maximum force of $\boldsymbol{\mathcal{F}}_{\max,x} = 140\,\mathrm{N}$. With these limits it is possible to allocate the generation of the desired force $\boldsymbol{\mathcal{F}}_{\mathrm{set},x}$ equally to $\boldsymbol{C}_{11}$ and $\boldsymbol{p}_{\mathrm{set},x}$ as follows:

$$\boldsymbol{p}_{\mathrm{set},x} = \boldsymbol{p}_{\mathrm{meas},x} - \mathrm{sign}\left(\boldsymbol{\mathcal{F}}_{\mathrm{set},x}\right)\sqrt{\frac{\boldsymbol{\mathcal{F}}_{\mathrm{set},x}}{\boldsymbol{\mathcal{F}}_{\max,x}}}\Delta x_{\max}\lambda \tag{2}$$

$$\boldsymbol{C}_{11} = \sqrt{\frac{\boldsymbol{\mathcal{F}}_{\mathrm{set},x}}{\boldsymbol{\mathcal{F}}_{\max,x}}}\boldsymbol{C}_{11,\max}\frac{1}{\lambda} \tag{3}$$

Here, $\lambda \in (0,1]$ is an optional design factor allowing for adjusting the trade-off between higher stiffnesses and larger deviations of the set-point to the measured one. Inserting (2) and (3) as well as their analogues for the remaining DOFs into (1) yields the validity of the approach.

B. Generation of wrench set-values

While (2) and (3) can be used to compute stiffnesses and set-points for wrenches of any origin, they often depend on the pose of the HMI and thus the current commanded values. This is for example the case if certain commanded values are to be avoided e.g. to prevent a collision of the operated robotic asset or to generate a general haptic experience for the operator like e.g. snaps to certain poses.

In these scenarios, we found it particularly useful to consider potential fields $\boldsymbol{\Phi}\left(\boldsymbol{p}\right) : \mathbb{R}^6 \rightarrow \mathbb{R}$ to generate the set-values for the wrenches. Doing so allows to compress the problem of assigning each pose of the robotic arm a vector of set-values for wrenches to only assigning each pose a value, which makes visualization and design more transparent in many cases. The set-values for the wrenches in each pose of the workspace can then be obtained by computing the gradient field of $\boldsymbol{\Phi}$:

$$\boldsymbol{\mathcal{F}}_{\mathrm{set}}\left(\boldsymbol{p}\right) = \mathrm{grad}(\boldsymbol{\Phi}\left(\boldsymbol{p}\right)) \tag{4}$$

Please note that $\boldsymbol{\Phi}$ can be time-variant to generate dynamic haptic experiences for the operator.

C. Optimal initial configuration

During the dynamic behaviour described before, the kinematic redundancy of the LBR is used to avoid the joint limits as well as singularities that would restrict the movement of the HMI through nullspace motion. The distance from singularities is termed manipulability [26] and forms a key aspect for the application of a kinematic machine as HMI. While the pose of the LBR is mainly influenced by the operator during use, the initial pose can be freely chosen within ergonomically feasible limits. Hence, to ensure the best manipulability possible, we compute the pose of optimal

manipulability to subsequently utilize it as initial pose of the HMI. To do so, we consider the manipulability measure μ of [27]:

$$\mu = \sqrt{\det\left(\boldsymbol{J}\boldsymbol{J}^\top\right)} \tag{5}$$

Here, $\boldsymbol{J}$ denotes the Jacobian matrix of the first-order differential kinematics [26]. As the redundant seventh axis only improves manipulability, we continue to consider the pose of optimal manipulability for the remaining six joints of the LBR. For six joints, $\boldsymbol{J}$ is a square matrix, hence $\det(\boldsymbol{J}) = \det(\boldsymbol{J}^\top)$. Using the multiplication property of the determinant $\det\left(\boldsymbol{J}\boldsymbol{J}^\top\right) = \det\left(\boldsymbol{J}\right)\det\left(\boldsymbol{J}^\top\right)$ yields:

$$\mu = \left|\det\left(\boldsymbol{J}\right)\right| \tag{6}$$

Defining $\boldsymbol{J}$ as in [26] and [28], (6) can be analytically expressed as:

$$\mu = \left|k_{\text{kin}}\sin(\theta_2)\sin(\theta_4)\cos(\theta_5)\right| \tag{7}$$

Here, $\theta_i, i \in \{1, ..., 6\}$ are the joint angles of the LBR and the factor k_{kin} denotes a constant depending only on the dimensions of the robotic arm. The maximum manipulability is hence achieved if

$$\theta_2 = (2n_1+1)\frac{\pi}{2}, \quad \theta_4 = (2n_2+1)\frac{\pi}{2}, \quad \theta_5 = n_3\pi \tag{8}$$

holds with $n_1, n_2, n_3 \in \mathbb{Z}$. Considering the joint limits as well as the distance to them, we get the following conditions for a pose with optimal manipulability:

$$\theta_2 = \pm\frac{\pi}{2}, \quad \theta_4 = \pm\frac{\pi}{2}, \quad \theta_5 = 0 \tag{9}$$

Only joints 2, 4 and 5 affect the pose of optimal manipulability, the other joint angles can be set arbitrarily. The optimal initial configuration used in the experiments is determined by ergonomic considerations and shown in Fig. 1.

IV. Evaluation and Applications

We ran numerous tests using the HMI to operate simulated drones, mobile robot platforms and ground robots as well as real ground robots, a real mobile robot platform and a real miniature robotic arm. Here, we exemplarily report on a comparative study depicted in Fig. 3a and the two applications shown in Fig. 3b and Fig. 3c.

A. Comparative Study

To evaluate whether the proposed system is able to be used as an input device, we performed a study with 20 participants (17 male, 3 female, 17 in their twenties, all of them operating with their right hand) comparing it to a state of the art Brunner CLS-E Joystick with two degrees of freedom and up to $4.2\,\text{Nm}$ of haptic feedback.

1) Setup: To compare the two HMIs, the workspace of the LBR HMI was limited to the x- and y-DOF, matching the workspace of the Brunner CLS-E with $160\text{mm}\times160\text{mm}$. The inputs of both HMIs were linearly mapped to the position of a cross on the screen in front of the participants. The participants were given the task to move the position of the cross to a displayed goal position. During the study, this goal position was discretely switched and the resulting input trajectories were recorded. Each participant used five HMI configurations in five measurement phases; before each measurement phase a training phase took place where the participants familiarized themselves with the system they then used during the measurement phase. Only data from measurement phases was used for evaluation. The five input configurations were (C1) LBR HMI w/o automation support, (C2) LBR HMI with automation support, (C3) Brunner CLS-E w/o automation support, (C4) Brunner CLS-E with automation support and (C5) LBR HMI with an increased workspace of $320\text{mm}\times320\text{mm}$. The supporting automation was implemented as impedance control around the goal state, its stiffness was tuned such that a residual distance from the goal state of approximately 15% of the workspace remained without an operator. The order of the usage of either the LBR HMI or the Brunner CLS-E was randomized to account for possible overarching learning effects outside of the training phases; 10 participants started with the LBR HMI, 10 started with the Brunner CLS-E, respectively. The main focus of the study is to compare C1-C4. Here each measurement phase consisted of 15 switches of the goal state in intervals ranging from $5\,\text{s}$ to $10\,\text{s}$. To avoid fatigue of the participants, the duration of the experiment had to be limited, hence C5 was only evaluated on a goal sequence of length three. The goal pattern was mirrored and rotated for each phase to prevent the participants form recognizing the pattern while

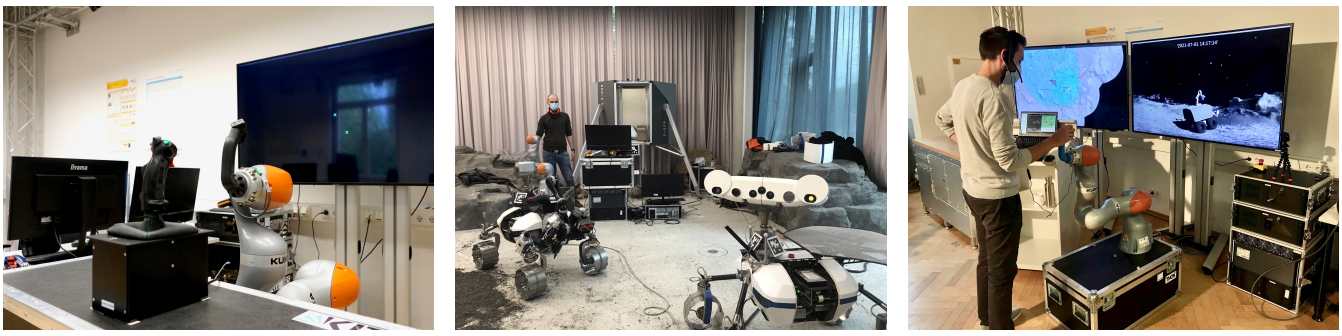

(a) Setup of the comparative study. (b) Setup of the ARCHES experiment. (c) Setup of the MIRACLES experiment.

Fig. 3: Real-world applications of the HMI.

still allowing for a direct comparison of the measurements. After each measurement phase, the participants filled out a questionnaire rating their mental load and their perceived performance on a scale of zero to 21.

2) Results: Fig. 4a depicts the mental loads reported by the participants, Fig. 4b shows the perceived performance ratings for C1-C4. The results with and without automation are pairwise comparable for both HMIs thus indicating that the proposed system is able to serve as HMI. They further underline the benefit of haptic support by an automation: The participants reported a decreased mental load and an increased perceived performance for both HMIs. The slightly lower perceived performance for C1 is probably due to the slightly lower agility of the LBR HMI compared to the Brunner CLS-E. The input measurements support this assertion. When evaluating the whole timeseries of N measurements $\boldsymbol{u}$ with respect to the goal inputs $\boldsymbol{u}_{\mathrm{goal}}$ using

$$\Delta_{\mathrm{RMSE}} = \sqrt{\frac{1}{N}\sum_{i=1}^{N} \left\|\boldsymbol{u}_{\mathrm{goal}} - \boldsymbol{u}\right\|^2}, \tag{10}$$

the average errors given in Table II result. The slightly slower regulation of errors due to goal switches with C1 and C2 compared to C3 and C4 leads to increased Δ_{RMSE} values. Nevertheless, using C2 allows for achieving slightly better performance than the much more agile C3.

Focusing on movements within a radius of 10% of the workspace size around the goal that require less agility but more precision yields the errors in Fig. 4c. They show a more uniform performance among the configurations with C2 even surpassing C3 and C4 slightly, indicating the suitability of the LBR HMI for high-precision tasks with lower agility requirements. The averages of the performance measure depicted in Fig. 4c strongly correlate ($\rho = -0.9889$) with the averages of the questionnaire results of Fig. 4b. This hints at the participants evaluating their performance more on the fine tuning around the goal than the movement towards it.

Due to time constraints C5 was evaluated and compared on an additional goal sequence of three goals that was only performed with C1, C3 and C5. The average errors within a radius of 10% of the workspace size around the goal are depicted in Fig. 4d. The results indicate an improvement of performance of C5 compared to C1 almost reaching the performance of C3. This is plausible as the larger workspace reduces input sensitivity, hence making precision tasks easier.

Overall this study shows that using an LBR as HMI is possible, underlines the benefits of force feedback and indicates that especially in precision tasks with medium to low agility requirements its performance might even surpass established HMI devices. The flexiblity of adjusting the workspace is also a promising feature for precision tasks.

TABLE II: Average Δ_{RMSE} error for C1 to C4 considering all participants and the entire measurement phases.

C1	C2	C3	C4
0.2567	0.2184	0.2260	0.1643

B. Teleoperation in ARCHES

The first application examines the teleoperation of the pan-tilt unit (PTU) of a Lightweight Rover Unit (LRU) [29] as a part of the ARCHES mission [30] depicted in the front right of Fig. 3b. The two DOFs pan-angle α and tilt-angle β are linearly mapped to the x- and y-DOFs of the HMI, respectively. Apart from limiting the workspace to a square of $35\,\mathrm{cm} \times 35\,\mathrm{cm}$, no force feedback was applied via the HMI. The resulting movement of the PTU after mapping the raw values to command values and communicating them via ROS is depicted in Fig. 5a. The evolution of the measured tilt-angle β_{m} of the PTU follows the tilt-angle β_{set} commanded via the HMI precisely, demonstrating that the HMI is capable of operating under real-world conditions.

C. Teleoperation in MIRACLES

The second application considers the teleoperation of robot Scout Rover [31] as a part of the MIRACLES mission [30]. Over the course of the mission, the LBR HMI was used twice for three days each with durations of up to 13 hours without faults, not including countless operating hours during mission preparation, thus demonstrating its reliability.

The commanded rover features velocity commands in one translational and one rotational DOF, which are mapped to the x- and y-DOFs of the HMI. Due to safety reasons, the simultaneous commanding of both a significant rotational and a significant translational movement had to be avoided to ensure proper vision with the front-facing camera of Scout Rover. To support the operator in complying with this rule via haptic feedback, we used the following potential field:

$$\Phi(x, y) = c_1 x^2 y^2 - c_2 \exp\left(-c_3\left(x^2 + y^2\right)\right) \tag{11}$$

Here, c_1, c_2 and c_3 are positive design parameters, x and y are considered displacements from the initial position. The first summand of (11) creates a gradient field counteracting movements in directions where both a translational and rotational command would result. The second summand creates a zone of attraction around the initial position to make it easier to command velocities of exactly zero. Fig. 5b depicts this potential field in the workspace of the HMI. To demonstrate the effect of the potential field, the operator was asked to command values in all DOF like they would do during operation. Subsequently, they were asked to move the handle randomly. Fig. 5c depicts the resulting trajectories. During nominal operation the potential field enables moving the handle in straight lines along the DOFs. The trajectory of the random movement shows how the wrenches are able to maintain a pose within the desired workspace, supporting the operator by doing so.

To relieve the operator from workload, a path-following automation was implemented to automatically follow pre-planned paths. Through an additional potential field overlay, (11) was manipulated to create a minimum at the command value computed by the path-following automation. Hence, the HMI was automatically moved to this command value.

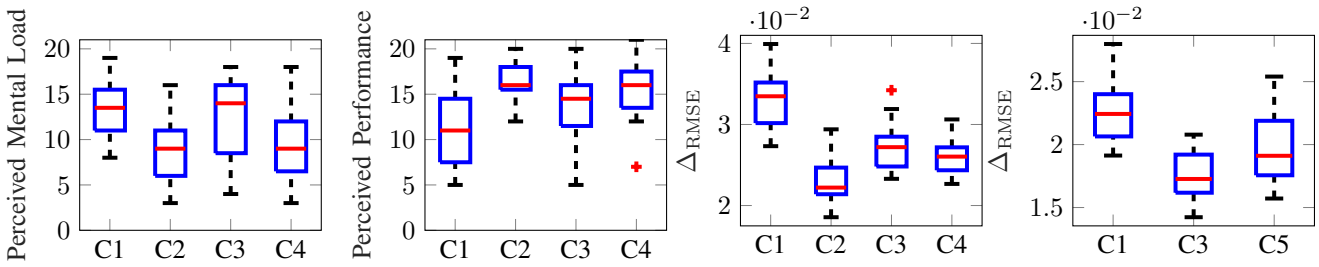

(a) Questionnaire results of perceived mental load.

(b) Questionnaire results of perceived performance.

(c) Measured performance for regulation task close to the goal.

(d) Measured performance for regulation task close to the goal.

Fig. 4: Results of the comparative study (C1 = LBR HMI w/o automation, C2 = LBR HMI with automation, C3 = Brunner CLS-E w/o automation, C4 = Brunner CLS-E with automation, C5 = LBR HMI w/o automation but larger workspace).

While this does allow for a fully automatic operation of the rover, the operator was able to intervene at any point by overruling the force of the automation overlay. This was necessary as the paths were only planned on a coarse map, hence the operator e.g. had to take over control to avoid obstacles that were unknown during planning.

Fig. 5d shows such a hand-over scenario where the operator created a deviation between the actually commanded values u_{trans} and u_{rot} and the commands intended by the path-following automation $u_{\mathrm{trans,A}}$ and $u_{\mathrm{rot,A}}$ by overruling the guiding force. First, the automation commands a constant translational speed of the Scout Rover. The operator detects an obstacle after 20 s and slows the rover down to perform a point-turn. This leads to a reaction of the path-following automation that now aims at compensating the rotational movement of the operator as it is unaware of the obstacle. The operator experiences this as a force pointing towards the new set-points. This effect increases while the operator performs a translational movement at 28 s. After finishing the movement, the operator rotates the rover towards the nearest point on the path segment, handing off to the automation at 53 s. After the automation starts a translational movement, the operator increases the commanded velocity for 5 s beyond the velocity intended by the automation to progress more quickly. Afterwards, the automation proceeds to follow the path. This application showcases the ability of the HMI to facilitate active cooperative operation concepts through wrenches.

V. CONCLUSION AND OUTLOOK

In this paper we demonstrate that a collaborative robotic arm can be used as an HMI. The proposed setup and control concept as well as the connection to ROS allow for a flexible use in a variety of scenarios with various operated robotic assets. The experiments reported in this work underline the applicability of the HMI to real-world teleoperation tasks highlighting its precision, reliability, and performance both with and without actively supporting the operator.

HUMAN SUBJECT DATA

All experiments were conduced in a safe and responsible manner and the operators and participants consented for the data to be used for anonymous publication.

ACKNOWLEDGMENT

The authors would like to thank Julian Schneider of the Karlsruhe Institute of Technology, Florian Steidle and Roy Lichtenheldt of the German Aerospace Center, Thorsten Graber of the European Space Agency as well as their respective teams for the pleasant collaboration on the experiments reported in this paper.

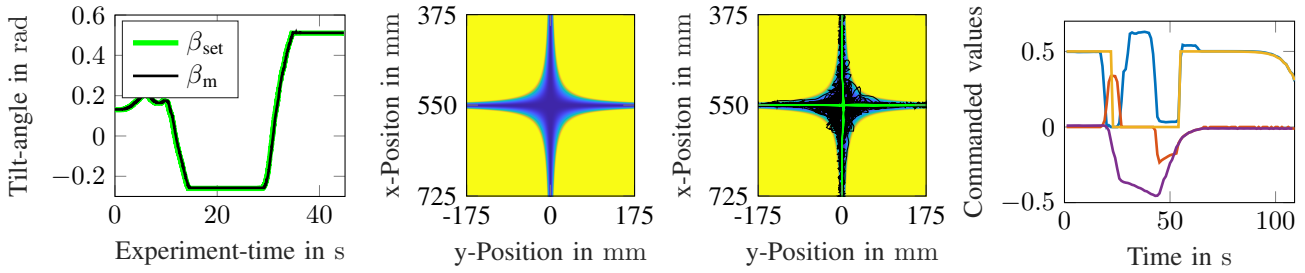

(a) Set and measured tilt-angle.

(b) Potential field over HMI workspace.

(c) Measured trajectories in — nominal operation and — random movement.

(d) Cooperation between operator and automation: — u_{trans}, — u_{rot}, — $u_{\mathrm{trans,A}}$, — $u_{\mathrm{rot,A}}$.

Fig. 5: Results of the ARCHES and MIRACLES applications.

REFERENCES

[1] J. Woerner, B. Foing, and Moon Village International Support Group, "The "Moon Village" Concept and Initiative," in *Annual Meeting of the Lunar Exploration Analysis Group*, 2016. [Online]. Available: https://www.hou.usra.edu/meetings/leag2016/pdf/5084.pdf

[2] N. Labeaga-Martínez, M. Sanjurjo-Rivo, J. Díaz-Álvarez, and J. Martínez-Frías, "Additive manufacturing for a Moon village," *Procedia Manufacturing*, vol. 13, pp. 794–801, 2017.

[3] C. Heinicke and B. Foing, "Human habitats: Prospects for infrastructure supporting astronomy from the Moon: Human support to astronomy from the Moon," *Philosophical Transactions of the Royal Society A: Mathematical, Physical and Engineering Sciences*, 2021.

[4] B. H. Foing, "Reaction: Surviving on the Moon, Mars, and Asteroids," *Chem*, vol. 4, no. 1, pp. 14–15, 2018.

[5] A. Wedler, M. Wilde, J. Reill, M. J. Schuster, M. Vayugundla, S. G. Brunner, K. Bussmann, A. Dömel, M. Drauschke, H. Gmeiner, H. Lehner, P. Lehner, M. G. Müller, W. Stürzl, R. Triebel, B. Vodermayer, A. Börner, R. Krenn, A. Dammann, U.-C. Fiebig, E. Staudinger, F. Wenzhöfer, S. Flögel, S. Sommer, T. Asfour, M. Flad, S. Hohmann, M. Brandauer, and A. O. Albu-Schäffer, "From single autonomous robots toward cooperative robotic interactions for future planetary exploration missions," in *Proceedings of the International Astronautical Congress, IAC*, 2018.

[6] B. A. Lehner, D. G. Mazzotta, L. Teeney, F. Spina, A. Filosa, A. C. Pou, J. Schlechten, S. Campbell, and P. L. Soriano, "Human Assisted Robotic Vehicle Studies - A conceptual end-to-end mission architecture," *Acta Astronautica*, vol. 140, pp. 380–387, 2017.

[7] D. Coutinho and C. Welch, "Interface standardization for the moon village," in *Proceedings of the International Astronautical Congress, IAC*, 2018.

[8] B. Sherwood, "Principles for a practical Moon base," *Acta Astronautica*, vol. 160, pp. 116–124, 2019.

[9] T. Krueger, E. Ferreira, A. Gherghescu, L. Hann, E. den Exter, F. van der Hulst, L. Gerdes, L. Cencetti, A. Pereira, H. Singh, M. Panzirsch, T. Hulin, R. Balachandran, B. Weber, and N. Lii, "Designing and testing a robotic avatar for space-to-ground teleoperation: The developers' insights," in *Proceedings of the International Astronautical Congress, IAC*, 2020.

[10] Astrobotic Technology, "Peregrine Lunar Lander Payload User's Guide," 2020. [Online]. Available: https://www.astrobotic.com/wp-content/uploads/2021/01/Peregrine-Payload-Users-Guide.pdf

[11] M. Kyrarini, F. Lygerakis, A. Rajavenkatanarayanan, C. Sevastopoulos, H. R. Nambiappan, K. K. Chaitanya, A. R. Babu, J. Mathew, and F. Makedon, "A Survey of Robots in Healthcare," *Technologies*, vol. 9, no. 1, p. 8, 2021.

[12] G. A. Zachiotis, G. Andrikopoulos, R. Gornez, K. Nakamura, and G. Nikolakopoulos, "A Survey on the Application Trends of Home Service Robotics," in *Proceedings of the 2018 IEEE International Conference on Robotics and Biomimetics, ROBIO*, 2018, pp. 1999–2006.

[13] E. Matheson, R. Minto, E. G. Zampieri, M. Faccio, and G. Rosati, "Human-robot collaboration in manufacturing applications: A review," *Robotics*, vol. 8, no. 4, pp. 1–25, 2019.

[14] KUKA Deutschland GmbH, "LBR iiwa 7 R800, LBR iiwa 14 R820 Specification," 2019.

[15] 3D Systems, "Phantom Premium - Advanced haptic devices for academic and commercial research and development," 2016. [Online]. Available: https://de.3dsystems.com/sites/default/files/2017-02/3DSystems-Haptics-PhantomPremium_2P_EN_Letter_WEB.pdf

[16] Force Dimension, "Sigma.7 Haptic Device," 2019. [Online]. Available: https://www.forcedimension.com/images/doc/specsheet_-_sigma7.pdf

[17] Y. Tsumaki, H. Naruse, D. N. Nenchev, and M. Uchiyama, "Design of a compact 6-dof haptic interface," in *Proceedings of the 1998 IEEE International Conference on Robotics and Automation*, 1998, pp. 2580–2585.

[18] J. Yoon and J. Ryu, "Design, fabrication, and evaluation of a new haptic device using a parallel mechanism," *IEEE/ASME Transactions on Mechatronics*, vol. 6, no. 3, pp. 221–233, 2001.

[19] D. Ryu, J.-B. Song, C. Cho, S. Kang, and M. Kim, "Development of a six DOF haptic master for teleoperation of a mobile manipulator," *Mechatronics*, vol. 20, no. 2, pp. 181–191, 2010.

[20] H. Iwata, "Artificial reality with force-feedback: Development of desktop virtual space with compact master manipulator," *ACM SIGGRAPH Computer Graphics*, vol. 24, no. 4, p. 165–170, 1990.

[21] S. S. Lee and J. M. Lee, "Design of a general purpose 6-dof haptic interface," *Mechatronics*, vol. 13, no. 7, pp. 697–722, 2003.

[22] M. H. Vu and U. J. Na, "A new 6-dof haptic device for teleoperation of 6-dof serial robots," *IEEE Transactions on Instrumentation and Measurement*, vol. 60, no. 11, pp. 3510–3523, 2011.

[23] International Organization for Standardization, "ISO/TS 15066 Robots and robotic devices — Collaborative robots," 2016.

[24] M. Quigley, B. Gerkey, K. Conley, J. Faust, T. Foote, J. Leibs, E. Berger, R. Wheeler, and A. Ng, "Ros: an open-source robot operating system," in *Proceedings of the IEEE International Conference on Robotics and Automation (ICRA) Workshop on Open Source Robotics*, Kobe, Japan, 2009.

[25] M. Safeea and P. Neto, "KUKA Sunrise Toolbox: Interfacing Collaborative Robots with MATLAB," *IEEE Robotics and Automation Magazine*, vol. 26, no. 1, pp. 91–96, 2019.

[26] S. Chiaverini, G. Oriolo, and A. A. Maciejewski, "Redundant Robots," in *Springer Handbook of Robotics*, 2nd ed., B. Siciliano and O. Khatib, Eds. Cham: Springer International Publishing, 2016, ch. 10, pp. 221–240.

[27] T. Yoshikawa, "Manipulability of Robotic Mechanisms," *The International Journal of Robotics Research*, vol. 4, no. 2, pp. 439–446, 1985.

[28] J. Denavit and R. S. Hartenberg, "A Kinematic Notation for Lower-Pair Mechanisms Based on Matrices," in *Annual Meeting of the American Society of Mechanical Engineers*, New York, 1954, pp. 215–221.

[29] M. J. Schuster, S. G. Brunner, K. Bussmann, S. Büttner, A. Dömel, M. Hellerer, H. Lehner, P. Lehner, O. Porges, J. Reill, S. Riedel, M. Vayugundla, B. Vodermayer, T. Bodenmüller, C. Brand, W. Friedl, I. Grixa, H. Hirschmüller, M. Kaßecker, Z. C. Márton, C. Nissler, F. Ruess, M. Suppa, and A. Wedler, "Towards Autonomous Planetary Exploration: The Lightweight Rover Unit (LRU), its Success in the SpaceBotCamp Challenge, and Beyond," *Journal of Intelligent and Robotic Systems: Theory and Applications*, vol. 93, no. 3-4, pp. 461–494, 2019.

[30] M. J. Schuster, M. G. Muller, S. G. Brunner, H. Lehner, P. Lehner, R. Sakagami, A. Domel, L. Meyer, B. Vodermayer, R. Giubilato, M. Vayugundla, J. Reill, F. Steidle, I. Von Bargen, K. Bussmann, R. Belder, P. Lutz, W. Sturzl, M. Smisek, M. Moritz, S. Stoneman, A. F. Prince, B. Rebele, M. Durner, E. Staudinger, S. Zhang, R. Pohlmann, E. Bischoff, C. Braun, S. Schroder, E. Dietz, S. Frohmann, A. Borner, H. W. Hubers, B. Foing, R. Triebel, A. O. Albu-Schaffer, and A. Wedler, "The ARCHES Space-Analogue Demonstration Mission: Towards Heterogeneous Teams of Autonomous Robots for Collaborative Scientific Sampling in Planetary Exploration," *IEEE Robotics and Automation Letters*, vol. 5, no. 4, pp. 5315–5322, 2020.

[31] R. Lichtenheldt, E. Staudinger, S. Adeli, J. Vera, G. Giudice, and M. Baqué, "A mission concept for lava tube exploration on mars and moon – the dlr scout rover." in *52nd Lunar and Planetary Science Conference*, 2021.